Nicotinic Receptor Fourth Transmembrane Domain
Hydrogen Bonding by Conserved Threonine Contributes to Channel Gating Kinetics

Cecilia Bouzat,* Francisco Barrantes,* and Steven Sine‡

From the From the *Instituto de Investigaciones Bioquímicas, Universidad Nacional del Sur-Consejo Nacional de Investigaciones Científicas y Técnicas, 8000 Bahía Blanca, Argentina; and ‡Receptor Biology Laboratory, Department of Physiology and Biophysics, Mayo Foundation, Rochester, Minnesota 55905

abstract The fourth transmembrane domain (M4) of the nicotinic acetylcholine receptor (AChR) contributes to the kinetics of activation, yet its close association with the lipid bilayer makes it the outermost of the transmembrane domains. To investigate mechanistic and structural contributions of M4 to AChR activation, we systematically mutated αT422, a conserved residue that has been labeled by hydrophobic probes, and evaluated changes in rate constants underlying ACh binding and channel gating steps. Aromatic and nonpolar mutations of αT422 selectively affect the channel gating step, slowing the rate of opening two- to sevenfold, and speeding the rate of closing four- to ninefold. Additionally, kinetic modeling shows a second doubly liganded open state for aromatic and nonpolar mutations. In contrast, serine and asparagine mutations of αT422 largely preserve the kinetics of the wild-type AChR. Thus, rapid and efficient gating of the AChR channel depends on a hydrogen bond involving the side chain at position 422 of the M4 transmembrane domain.

key words: patch clamp • kinetic analysis • nicotinic acetylcholine receptor channel gating • fourth transmembrane domain • hydrogen bond

INTRODUCTION

The nicotinic acetylcholine receptor (AChR)[1] is a pentamer of homologous subunits with composition $\alpha_2\beta\gamma\delta$ in fetal muscle and $\alpha_2\beta\epsilon\delta$ in the adult. Each subunit contains an amino-terminal extracellular domain of ~210 amino acids, four transmembrane domains (M1–M4), and a short extracellular carboxy-terminal tail. The M2 domain of each subunit contributes to the cation-selective channel, and agonist binding triggers motion of M2 to initiate ion flow (Unwin, 1995). The locations and functional roles of the M1, M3, and M4 transmembrane domains are not as well understood. The M1 domain appears closely associated with both the ion conducting pathway and the bilayer, as revealed by substituted cysteine accessibility and labeling by hydrophobic reagents (Akabas and Karlin, 1995; Blanton and Cohen, 1994). The M3 domain has been shown to have some contact with lipid (Blanton and Cohen, 1994) and to contribute to channel opening and closing rates (Wang et al., 1999). The M4 domain is the least conserved among the transmembrane domains, is the most hydrophobic, and has been extensively labeled by hydrophobic probes (Blanton and Cohen, 1992, 1994), suggesting that it is the outermost of the transmembrane domains. Labeling by the photoactivatable hydrophobic probe [^{3}H]TID {[^{3}H]3-(trifluoromethyl)3-m-(iodophenyl)diazirine} occurs at C412, M415, C418, T422, and V425 of the α subunit of *Torpedo californica* AChR, making these the best candidates for residues in contact with the lipid bilayer (Blanton and Cohen, 1994). Mutagenesis studies suggest that the M4 domain is essential for proper AChR activation (Lee et al., 1994; Ortiz-Miranda et al., 1997). By alanine scanning of the lipid-exposed residues in the M4 domain of the α subunit, we recently showed that T422 affects channel open duration (Bouzat et al., 1998).

Here we examine the structural and mechanistic contributions of the M4 domain to AChR activation by systematically mutating αT422 of the mouse muscle AChR and evaluating changes in activation kinetics. Our results show that αT422 contributes through a hydrogen bond to both opening and closing steps.

MATERIALS AND METHODS

Construction of Mutant Subunits

Mouse cDNAs were used subcloned into the cytomegalovirus-based expression vector pRBG4 (Sine, 1993). Mutant α subunits were constructed by bridging the naturally occurring sites BstX-1 and BspM-1 with synthetic double-stranded oligonucleotides (Bio-Synthesis Inc.), essentially as described previously (Bouzat et al., 1998). Single-stranded oligonucleotides were purified by PAGE

Address correspondence to Cecilia Bouzat, Instituto de Investigaciones Bioquímicas, UNS-CONICET, Camino La Carrindanga Km 7, 8000 Bahía Blanca, Argentina. Fax: 54-291-4861201; E-mail: inbouzat@criba.edu.ar

[1]*Abbreviations used in this paper:* AChR, nicotinic acetylcholine receptor; M4, fourth transmembrane domain.

and annealed before ligation. Restriction mapping and dideoxy sequencing on polyacrylamide gels confirmed all constructs.

Expression of AChR

Human embryonic kidney cells (HEK293) were transfected with α (wild-type or mutant), β, δ, and ε cDNAs using calcium phosphate precipitation at a subunit ratio of 2:1:1:1 for α:β:δ:ε, respectively, essentially as described previously (Bouzat et al., 1994, 1998). For transfections, cells at 40–50% confluence were incubated for 8–12 h at 37°C with the calcium phosphate precipitate containing the cDNAs in DMEM plus 10% fetal bovine serum. Cells were used for single-channel measurements 1 or 2 d after transfection.

Patch-Clamp Recordings

Recordings were obtained in the cell-attached configuration (Hamill et al., 1981) at a membrane potential of −70 mV and at 20°C. The bath and pipette solutions contained 142 mM KCl, 5.4 mM NaCl, 1.8 mM $CaCl_2$, 1.7 mM $MgCl_2$, and 10 mM HEPES, pH 7.4. Patch pipettes were pulled from 7052 capillary tubes (Garner Glass), to produce final resistances of 5–7 MΩ, and were coated with Sylgard (Dow Corning Corp.). Pipette concentrations of ACh ranged from 10 to 1000 μM. Single channel currents were recorded using an Axopatch 200 B patch-clamp amplifier (Axon Instruments, Inc.) and digitized at 94 kHz with a PCM adapter (VR-10B; Instrutech). Data were transferred to a computer using the program Acquire (Bruxton Corp.) and detected by the half-amplitude threshold criterion using the program TAC 3.0 (Bruxton Corp.) at a final bandwidth of 10 kHz. Open- and closed-time histograms were plotted using a logarithmic abscissa and a square root ordinate (Sigworth and Sine, 1987) and fitted to the sum of exponentials by maximum likelihood using the program TACFit (Bruxton Corp.). For each patch corresponding to a given ACh concentration, the number of opening events ranged from 4,000 to 10,000.

Open probability within clusters (P_{open}) was experimentally determined at each ACh concentration by calculating the mean fraction of time the channel is open within a cluster. The experimental P_{open} determinations were compared with theoretical dose–response curves calculated from either Scheme I or II, using the fitted rate constants in Table II.

Kinetic Analysis

At ACh concentrations >10 μM, clusters of openings corresponding to a single channel were identified as a series of closely spaced events preceded and followed by closed intervals greater than a specified duration; this duration was taken as the point of intersection of the predominant closed-time component and the succeeding component in the closed-time histogram. To minimize errors in assigning cluster boundaries at the lower ACh concentrations, we analyzed only recordings from patches with low channel activity. Only clusters containing >10 openings were considered for further analysis. In addition, any clusters showing double openings were rejected. For each recording, kinetically homogeneous clusters were selected based on their mean channel open duration and open probability distributions (Wang et al., 1997). For each cluster within a recording, we calculated the P_{open} and mean open duration and plotted their distributions. Histograms were constructed and fitted by a Gaussian function, which yielded a mean and a standard deviation for each distribution. Typically, the distributions contained a dominant, approximately Gaussian component and minor contributions of clusters with different properties. Clusters showing mean open duration and open probability values within 2 SD of the mean of the major component were selected and retained for the kinetic analysis. Typically, >80% of the clusters were selected. For each recording, mean values of open probability, and mean open and closed durations changed little after the selection procedure (see examples of selection results in Table I). The similarity of the evaluated parameters before and after selection indicates no qualitative changes in the dwell-time distributions due to the selection procedure. The resulting open and closed intervals, from single patches at several ACh concentrations, were analyzed according to a kinetic scheme using the program MIL (QuB suite, www.qub.buffalo.edu). In brief, MIL simultaneously fits recordings obtained at different ACh concentrations, and estimates rate constants in a kinetic scheme using a maximum likelihood method that corrects for missed events (Qin et al., 1996). We typically included recordings obtained at 10, 30, 50, 100, 200, and 300 μM ACh in the analysis of each mutant AChR. The dead time was typically 30 μs, but the fitted rate constants were stable over a range of dead times ranging from 18 to 40 μs (data not shown). Probability density functions of open and closed durations were calculated from the fitted rate constants and instrumentation dead time and superimposed on the experimental dwell-time histogram, as described by Qin et al. (1996). Calculated rate constants were accepted only if the resulting probability density functions reasonably superimposed upon the experimental open- and closed-duration histograms at all ACh concentrations. To check the final set of fitted rate constants, open and closed intervals were simulated according to Scheme I or II, using the program SIMU (QuB suite). Simulated channel events were analyzed and the resulting dwell times were fitted with the program MIL. The original rate constants were recovered with 10–15% accuracy. Comparison of the fits to different schemes was evaluated by the log likelihood ratio (LLR). For example, a LLR of 50 indicates that the probability of the model with the higher LL is e^{50} times more than that of the scheme with the lower LL (Salamone et al., 1999).

RESULTS

We previously examined the M4 transmembrane domain by alanine-scanning mutagenesis, and found that αT422 was unique in that its mutation markedly affected the rate of channel closing (Bouzat et al., 1998). To further examine the structural contribution of αT422 to AChR activation, we replaced it by polar (serine and asparagine), aromatic (tryptophan and tyrosine), and nonpolar amino acids (alanine, valine, and cysteine). Then we transfected HEK293 cells with either wild-type or mutant α plus wild-type β, ε, and δ subunit cDNAs and recorded single channel currents.

AChR channels were activated by a range of desensitizing concentrations of ACh (10–1,000 μM) to produce clear clusters of events corresponding to a single channel (Sakmann et al., 1980). Wild-type as well as mutant AChRs open in clusters of well-defined activation episodes at ACh concentrations >10 μM. Each activation episode begins with the transition of a single receptor from the desensitized to the activatable state and terminates by returning to the desensitized state (Fig. 1). For both wild-type and mutant AChRs, closed intervals within clusters become progressively briefer with increasing ACh concentration (Fig. 2). However,

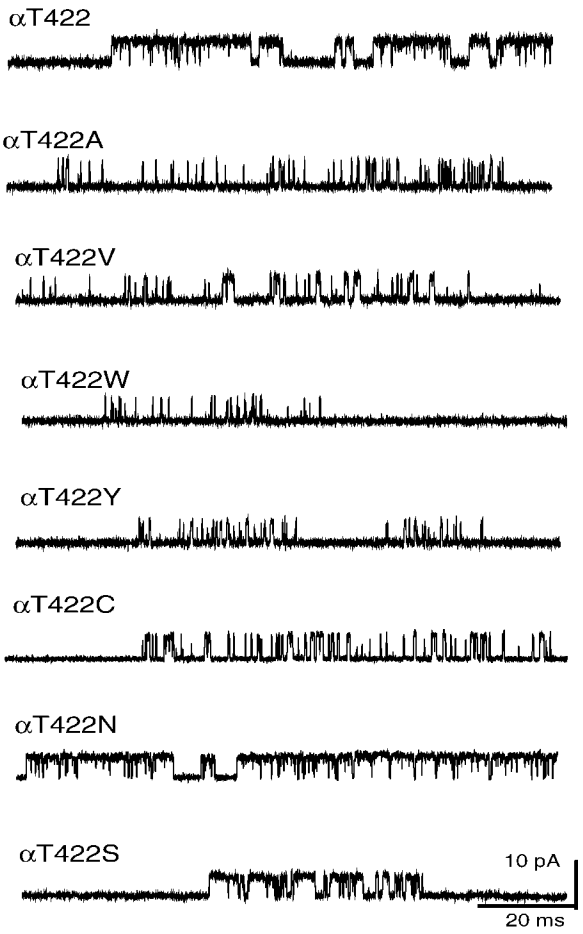

Figure 1. Clusters of single-channel currents from wild-type and mutant AChRs. Channels activated by 100 μM ACh were recorded from HEK cells expressing mouse wild-type ($\alpha_2\beta\epsilon\delta$) and mutant αT422A, αT422V, αT422W, αT422Y, αT422C, αT422N, and αT422S AChRs. Currents are displayed at a bandwidth of 9 kHz with channel openings as upward deflections. Membrane potential, −70 mV.

compared with wild-type, most of the mutant AChRs show both briefer openings and prolonged intracluster closings (Fig. 1).

For both wild-type and mutant AChRs, the predominant peak of the closed-time histograms moves to shorter duration with increasing ACh concentration (Fig. 2). However, for mutant AChRs containing alanine, closed intervals are clearly longer than those of wild-type AChRs at all ACh concentrations (Fig. 2). Similar results were obtained for receptors containing nonpolar (valine and cysteine) or aromatic (tryptophan and tyrosine) substitutions. The predominant open-time component of either wild-type or mutant AChRs does not change with changes in ACh concentration (Fig. 2). However for αT422A (Fig. 2), as well as for αT422V, αT422W, αT422Y, and αT422C AChRs (not shown), open-time distributions shift to briefer durations compared with wild-type AChRs. In contrast, when T422 is replaced by serine (Fig. 2) or asparagine (not shown), open- and closed-duration histograms are similar to those of wild type.

The observed changes in the kinetics of AChR activation could be due to changes in rate constants underlying either ACh binding or channel gating steps. To identify the kinetic steps affected by each M4 mutation, we fitted kinetic schemes to the open and closed dwell times. For wild-type AChRs, we used the classical activation scheme (Scheme I), where two agonists (A) bind to the receptor (R) in the resting state with association rates k_{+1} and k_{+2} and dissociate with rates k_{-1} and k_{-2}. Receptors occupied by one agonist open with rate β_1 and close with rate α_1, and AChRs occupied by two agonist molecules open with rate β_2 and close with rate α_2. At high agonist concentrations (>100 μM ACh) channel blockade is evident, requiring addition of the blocked state A_2B.

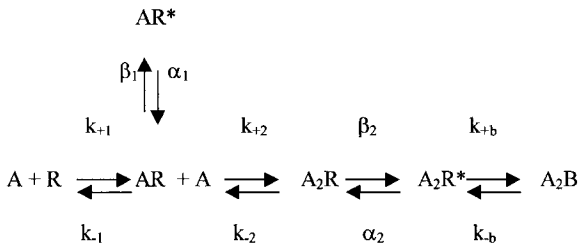

(SCHEME I)

To estimate the set of rate constants, Scheme I was fitted to the data using the program MIL (Qin et al., 1996). MIL computes the likelihood of the experimental series of open and closed times given a set of trial constants, and then changes the rate constants to maximize the likelihood. We simultaneously analyzed recordings obtained at multiple ACh concentrations (10–300 μM), with the aim of representing all the states in Scheme I in the fitting. The procedure for kinetic analysis requires selection of clusters to produce kinetically homogeneous data (MIL, QUB suite; Salamone et al., 1999). For each recording, kinetic homogeneity was determined by computing the mean channel open duration and open probability of each cluster, and then plotting their distributions. Only clusters showing P_{open} and mean open duration values within the mean ±2 SD were included in the subsequent analysis. Comparison of distributions before and after selection (see examples in Table I) indicates that the selected clusters are representative of the entire population of events for each recording. In addition, open- and closed-time histograms constructed with selected data are very similar to those constructed with the original events (not shown). Data of open and closed intervals corresponding to the selected clusters were subsequently used to fit Scheme I.

For wild-type AChR, β_2 was constrained to its known value (Sine et al., 1995; Wang et al., 1997; Salamone et

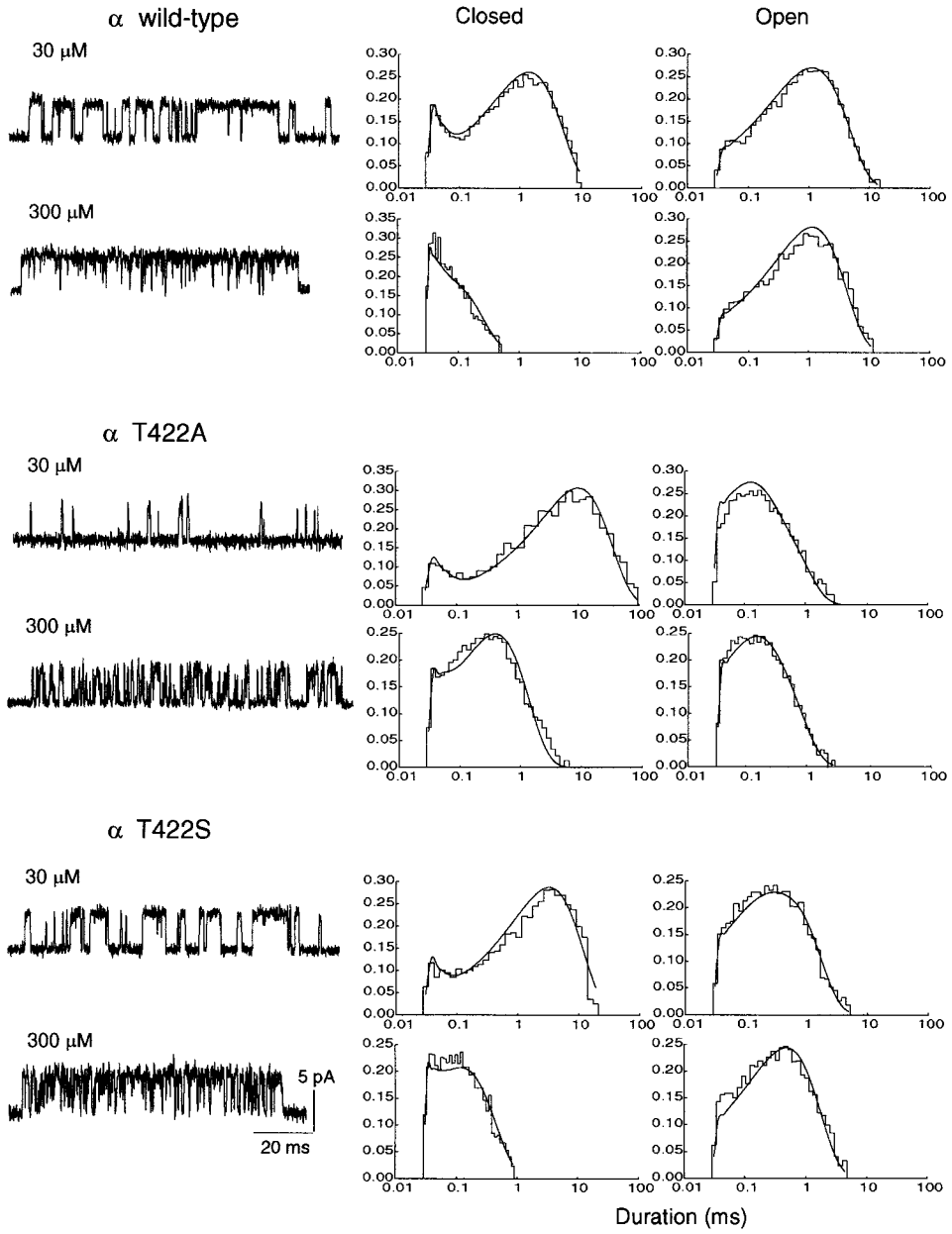

Figure 2. Kinetics of activation of wild-type and mutant AChRs. (Left) Channel traces corresponding to AChRs containing the indicated α subunit and activated by 30 and 300 μM ACh. Currents are displayed at a bandwidth of 9 kHz with channel openings as upward deflections. (Center and right) Closed- and open-time histograms with the fit for Scheme I (wild-type and αT422S) or Scheme II (αT422A) superimposed. Histograms were constructed with the selected clusters. The ordinate corresponds to the square root of the fraction of events per bin. Closed-time histograms are truncated to eliminate slow components due to desensitization.

al., 1999) because brief closings due to gating and channel blocking became indistinguishable at high ACh concentrations (Wang et al., 1997; Salamone et al., 1999). When β_2 was allowed to vary freely, MIL failed to converge to a well-defined set of rate constants and approached a value of ~100,000 s^{-1} (data not shown). Similar observations were recently reported by Salamone et al. (1999). Although channel blocking is too brief to be completely resolved with our instrumentation dead time of 30 μs, we retain channel block in Scheme I because significant numbers of blockages are resolved at our highest ACh concentrations of 300 μM. Moreover, the unblocking rate constant obtained under the present conditions is similar to values previously reported (Maconochie and Steinbach, 1995; Wang et al., 1997). Finally, association and dissociation rate constants were assumed to be equal at both binding sites, as previously described for adult mouse AChRs (Akk and Auerbach, 1996; Wang et al., 1997; Salamone et al., 1999).

Rate constant estimates obtained for wild-type AChR, shown in Table II, agree with those previously reported for mouse AChR (Wang et al., 1997; Salamone et al., 1999). The fitting analysis confirms that singly occupied AChRs open slowly and with low efficiency, but doubly occupied receptors open rapidly and efficiently.

We next applied kinetic analysis to AChRs containing mutations of αT422 using clusters selected as described for wild-type AChRs (Table I). Scheme I could not adequately describe data obtained from AChRs containing

TABLE I

Open Probability, Mean Open Duration, and Mean Closed Duration of Clusters of AChRs Containing α wild-type, αT422A, and αT422S Subunits

		P_{open}	Open duration	Closed duration	No. clusters	No. events
			ms	*ms*		
Wild type	Before	0.47 ± 0.07	1.05 ± 0.19	1.09 ± 0.16	32	12082
30 μM	After	0.47 ± 0.04	1.00 ± 0.09	1.12 ± 0.13	26	11086
Wild type	Before	0.93 ± 0.07	0.78 ± 0.30	0.06 ± 0.02	76	6398
300 μM	After	0.93 ± 0.02	0.79 ± 0.20	0.06 ± 0.01	70	6058
T422A	Before	0.02 ± 0.04	0.12 ± 0.03	16.5 ± 9.60	49	6136
30 μM	After	0.01 ± 0.01	0.12 ± 0.03	19.0 ± 6.50	42	3880
T422A	Before	0.31 ± 0.12	0.15 ± 0.06	0.35 ± 0.12	79	14240
300 μM	After	0.30 ± 0.10	0.14 ± 0.04	0.36 ± 0.12	73	13836
T422S	Before	0.11 ± 0.07	0.34 ± 0.18	3.05 ± 0.9	168	7804
30 μM	After	0.10 ± 0.04	0.33 ± 0.12	3.00 ± 0.8	157	7286
T422S	Before	0.77 ± 0.08	0.43 ± 0.19	0.12 ± 0.04	51	6346
300 μM	After	0.76 ± 0.07	0.38 ± 0.07	0.12 ± 0.12	43	5476

Values (mean ± SD) were obtained, before and after the selection procedure, from the open probability, mean channel open duration, and channel closed duration distributions of clusters corresponding to AChRs containing the indicated α subunit and activated by 30 and 300 μM ACh (recordings shown in Fig. 2). Clusters with mean values within ±2 SD of the mean were selected for kinetic analysis. Comparison of distributions before and after selection indicates that the final selected clusters are representative of the AChR in the patch. Similar results were obtained for all recordings (not shown).

the hydrophobic/aromatic mutations αT422A, αT422V, αT422Y, αT422W, and αT422C. Scheme I predicts a minor open-time component, associated with AR*, that decreases in relative area with increasing ACh concentration, but these mutant channels show two open components whose relative areas do not change with changes in ACh concentration. To account for two concentration-independent open-time components, we fitted Scheme II to dwell times from mutant AChRs. The classical activation scheme (Scheme I) is a subset of Scheme II, which has the opening step separated into two sequential steps. An alternative branched scheme, containing two open states connected to the A_2R closed state, also described the data, but was found to be less likely for all mutant AChRs, as judged by maximum likelihood analysis. For example, for the αT422A AChR, Scheme II was e^{110} times more likely than the branched scheme.

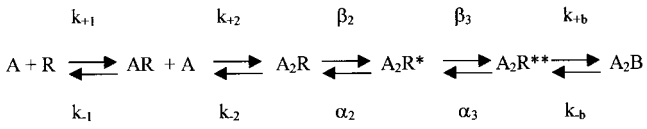

(SCHEME II)

In fitting Scheme II to data from AChRs containing hydrophobic or aromatic mutations, the two binding sites were assumed to have equal microscopic rate constants, as found for wild-type AChR. In contrast to fitting Scheme I to data from the wild type, it was possible to allow β_2 to vary freely. For the hydrophobic and aromatic mutations, the unblocking rate constant (k_{-b}) was constrained to the value used for wild-type AChRs because M4 does not contribute to the channel pore (Blanton and Cohen, 1994), and because we found the channel conductance to remain constant for all M4 mutations. The resulting fitting analysis establishes that the T422V, T422A, T422Y, T422W, and T422C mutations markedly affect the kinetics of channel gating (Table II). The steps primarily affected are channel opening and closing, with changes of two- to sevenfold in the opening rate (β_2 in Scheme II) and four- to ninefold in the closing rate (α_2) (Table II). Therefore, the doubly occupied mutant AChR opens with greater latency and reduced efficiency compared with wild-type AChRs. However, after opening, the mutant channels rapidly return to the closed state or, with low probability, reach a more stable open state, represented by A_2R^{**} in Scheme II.

In contrast to the hydrophobic and aromatic mutations, AChRs containing the serine or asparagine mutations could be well fitted by Scheme I (Fig. 2). Using the same constraints as in wild-type AChRs (β_2 = 49,000 s^{-1} and equivalent binding sites), the best-fit rate constants indicate that the primary effect of the serine and asparagine mutations is a twofold increase in the channel closing rate, α_2 (Table II). Because, as described above for wild-type AChRs, it was necessary to constrain β_2 in fitting data from αT422S and αT422N AChRs, and because the hydrophobic and aromatic mutations affected β_2, we systematically varied β_2 from 19,000 to 49,000 s^{-1}. Based on likelihood, the best description of the αT422S and αT422N data was obtained when β_2 was 49,000 s^{-1}, as found for wild-type AChR. For example, for the αT422S AChR, the fit using β_2 = 49,000 was e^{24}, e^{81}, and e^{235} times more likely than with β_2 equal to 39,000, 29,000, and 19,000 s^{-1}, respectively.

Although dwell times from the hydrophobic and aromatic mutants were not well described by Scheme I, dwell times from wild-type, αT422S, and αT422N AChRs could be well described by either Scheme I or Scheme II (Table II). To show that changes in rate constants due to the mutations are not scheme dependent, we also fitted Scheme II to data from wild-type as well as αT422S and αT422N AChRs (Table II). Comparison of log likelihoods, obtained after fitting both schemes to wild-type and αT422N data, reveals that Scheme I provides the better description; Scheme I is e^{75} and e^{170} times more likely than Scheme II for wild-type and T422N AChRs, respectively. On the other hand, for the αT422S mutation, Scheme II is e^{72} more likely than Scheme I. Fitting Scheme II to data from the serine and asparagine mutations reveals only slight changes in the gating steps, similar to results obtained with

TABLE II

Kinetic Parameters for Mouse Wild-Type and αT422 Mutant AChRs

	Scheme	k_{+1}	k_{-1}	k_{+2}	k_{-2}	β_1	α_1	β_2	α_2	θ_2	β_3	α_3	k_{+b}	k_{-b}
Wild type	1	360 ± 12	28700 ± 1200	180 ± 6	57400 ± 2300	560 ± 50	2300 ± 140	49000	1400 ± 30	35			9 ± 1	79000 ± 6000
T422S	1	260 ± 10	36770 ± 2100	130 ± 5	73500 ± 4200	690 ± 50	9100 ± 580	49000	3900 ± 100	12			9 ± 1	79000
T422N	1	220 ± 6	16000 ± 350	110 ± 3	32000 ± 700	3700 ± 190	4600 ± 130	49000	2900 ± 70	16			5 ± 1	79000
T422V	2	140 ± 10	27400 ± 1200	70 ± 5	54700 ± 2400			28100 ± 1700	8600 ± 750	3.2	758 ± 130	3400 ± 300	30 ± 4	79000
T422A	2	250 ± 10	27600 ± 1300	120 ± 5	55300 ± 2500			12800 ± 400	10400 ± 180	1.2	1430 ± 140	4900 ± 260	57 ± 5	79000
T422W	2	250 ± 20	30300 ± 2600	120 ± 10	60700 ± 5200			13600 ± 700	11150 ± 240	1.2	394 ± 70	1680 ± 250	166 ± 10	79000
T422Y	2	230 ± 30	25000 ± 3300	120 ± 14	50185 ± 6628			10550 ± 950	14700 ± 650	0.7	1470 ± 370	5306 ± 780	160 ± 33	79000
T422C	2	260 ± 20	16000 ± 800	130 ± 7	33000 ± 1700			6300 ± 130	5300 ± 100	1.2	2100 ± 160	3300 ± 140	18 ± 1	79000
Wild type	2	415 ± 9	27800 ± 800	210 ± 8	56000 ± 1500			49000	2300 ± 100	21	2000 ± 600	4600 ± 800	30 ± 8	99000 ± 8000
T422S	2	260 ± 8	31400 ± 1100	130 ± 4	63000 ± 2300			49000	6200 ± 150	8	850 ± 140	2900 ± 300	19 ± 4	99000
T422N	2	380 ± 6	16400 ± 320	190 ± 4	33000 ± 700			49000	5700 ± 100	9	610 ± 60	1400 ± 90	15 ± 2	99000

Rate constants are in units of $\mu M^{-1}\ s^{-1}$ for association rate constants and s^{-1} for all others. Values are results of a global fit of Schemes I and II to data obtained over the range 10–300 μM ACh, with standard errors. Data without showing standard error has been constrained to allow a better fit. The channel opening equilibrium constant, θ_2, is the ratio of the opening to closing rate constants corresponding to the major open state (β_2/α_2).

Scheme I (Table II). Comparison of wild-type and M4 mutant rate constants, calculated on the basis of Scheme II, also shows that αT422 contributes primarily to channel opening and closing, and that these steps are largely affected by the presence of hydrophobic or aromatic residues (Table II). Thus, residues preserving the hydrogen bonding ability of the original threonine support nearly normal gating kinetics.

The channel gating equilibrium constant, θ_2, calculated as β_2/α_2, significantly decreases in most of the mutants (Table II). For each side chain at position 422, we calculated the net free energy change for the gating equilibrium, as well as the activation free energy changes for opening and closing transitions (Table III). Free energy changes of ~2 kcal/mol in the gating equilibrium are observed when nonpolar or aromatic amino acids are substituted into position 422, whereas only slight changes occur when serine or asparagine are substituted. When threonine is replaced by either aromatic or nonpolar amino acids, the activation free energy for opening increases, whereas, for all mutants, activation free energy for closing decreases (Table III).

Rates of agonist association and dissociation (Table II) and dissociation equilibrium constants (Table IV) are not significantly affected by these mutations. Thus, T422 selectively affects channel opening and closing transitions.

To determine the overall consequences of each mutation for AChR activation, and to evaluate consistency of the fitted rate constants, we computed the open probability from the fitted rate constants and compared it

TABLE III

Differences in Free Energy of Channel Gating, and Open and Closing Reactions

Mutation	Gating $\Delta(\Delta G)$	Opening $\Delta(\Delta G)$	Closing $\Delta(\Delta G)$
	kcal/mol	*kcal/mol*	*kcal/mol*
T442S	0.6	0	−0.6
T442N	0.5	0	−0.4
T442V	1.4	0.3	−1.0
T442A	2.0	0.7	−1.2
T442W	2.0	0.7	−1.2
T442Y	2.3	0.8	−1.4
T442C	2.0	1.1	−0.8

Gating $\Delta(\Delta G)$ is the change between mutant (m) and wild-type (wt) AChRs in the energy of channel gating, calculated by $\Delta(\Delta G) = -RT\ln(\theta_2 m/\theta_2 wt)$ (where R is the gas constant and T is the absolute temperature). θ_2 is the initial channel opening equilibrium constant shown in Table II. $\Delta(\Delta G)$ is the change between mutant and wild-type AChRs in the energy that the channel must overcome to make the transition from the biliganded closed state to the main open state (Opening) and from this open to the closed state (Closing). The differences in free energies are calculated as $\Delta(\Delta G) = -RT\ln(\beta_2 m/\beta_2 wt)$ and $-RT\ln(\alpha_2 m/\alpha_2 wt)$ for opening and closing, respectively.

TABLE IV

Equilibrium Constants for Mouse Wild-Type and αT422 Mutant AChRs

	K_1	K_2
	μM	*μM*
Wild type	70	320
T422S	140	560
T422N	70	260
T422V	190	780
T422A	110	460
T422W	120	500
T422Y	100	410
T422C	62	260

Equilibrium constants were obtained with data from Table II. $K_1 = k_{-1}/k_{+1}$, $K_2 = k_{-2}/k_{+2}$.

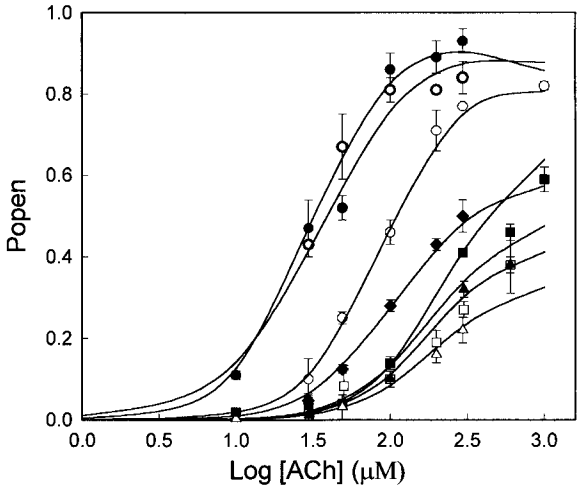

Figure 3. Agonist concentration dependence of the channel open probability. For AChRs containing the indicated α subunits, the mean fraction of time the channel is open during a cluster (Popen) was experimentally determined at the indicated concentrations of ACh. Each point corresponds to the mean ± SD of three to four patches. The curves were calculated from either Scheme I (αWT, αT422S, and αT422N) or Scheme II (αT422V, αT422A, αT422W, αT422Y, and αT422C), using the fitted rate constants in Table II, and superimposed on the P_{open} measurements. P_{open} curves corresponding to wild type, T422S, and T422N AChRs calculated from Scheme II are almost identical to those shown in the figure. ●, wild-type; bolded open circle, αT422N; ○, αT422S; ◆, αT422C; ■, αT422V; □, αT422A; ▲, αT422W; and △, αT422Y.

with the experimentally determined open probability (Fig. 3). For wild-type AChRs, open probability increases with increasing ACh concentration, reaching a maximum of ~0.9 at 100 μM and showing an EC_{50} of 40 μM (Fig. 3). For most mutant AChRs, both the EC_{50} and maximum open probability change. The open probability curves are shifted to higher ACh concentrations, owing to decreased efficiency of channel gating. For the mutants T422A, T422V, T422W, T422Y, and T422C, open probability is <0.6 at 1,000 μM, and the EC_{50} values range from 200 to 300 μM (Fig. 3). Thus, mutations of αT422 affect both efficacy and EC_{50} for AChR activation. As expected, the profile for the T422N mutant is similar to that of wild-type AChR, and only slight changes are observed when threonine is replaced by serine. The EC_{50} and maximum open probability values for the T422S mutant are 80 μM and 0.8, respectively (Fig. 3). The dose–response curves computed from the fitted rate constants closely follow the experimentally determined open probability determinations, demonstrating overall consistency of the data.

DISCUSSION

T422 of the M4 domain of the α subunit is presumed to be located at the lipid–protein interface, owing to its susceptibility to labeling by a hydrophobic probe (Blanton and Cohen, 1994). Although M4 is the least conserved of the four transmembrane domains, the high degree of conservation of T422 among subunits and species indicates that it might play a structural or functional role. We previously reported that among residues in M4, αT422 is the most sensitive to mutation, with the alanine substitution decreasing the mean open time fivefold (Bouzat et al., 1998). Here we elucidated both mechanistic and structural bases for the contribution of αT422 to channel gating. Kinetic analysis of mutant αT422 AChRs disclose relatively small contributions to steps governing ACh binding to the resting, closed state of the AChR, but reveals significant contributions to steps underlying channel opening and closing.

Kinetic analysis requires that open and closed dwell times correspond to a single AChR channel. Clusters of opening events, corresponding to activation of the AChR between desensitized periods, were clearly distinguished at ACh concentrations >10 and 30 μM for wild-type and mutant AChRs, respectively. Because only clusters containing a single open conductance level were considered for kinetic analysis, it is possible to unequivocally assign the dwell times to sojourns in open and closed states of a single AChR. In addition, the clustering behavior observed for all mutant AChRs clearly demonstrates that, like wild-type, they can undergo cycles of desensitization and resensitization in the continued presence of ACh.

Based on gatings kinetics, one can distinguish the polar serine and asparagine from the nonpolar or aromatic amino acid mutations at position 422 as follows. (a) Kinetic changes due to replacement of T422 by serine or asparagine: recordings obtained from these mutant AChRs are similar to those from wild-type AChRs (Fig. 1). Slight changes in the open- and closed-time histograms are observed (Fig. 2). Data can be well fitted by the classical description of activation for wild-type AChR. The only detectable change is a twofold in-

crease in the channel closing rate. (b) Kinetic changes due to replacement of αT422 by nonpolar or aromatic residues: recordings show very brief openings and prolonged closings. The classical activation scheme does not fit the experimental data. However, expanding the classical scheme to include two sequentially connected open states (Scheme II) satisfactorily describes the data. Kinetic analysis based on Scheme II reveals that the rate of opening to the first open state is slower than the analogous step in wild-type AChRs, but the closing rate from this state (α_2) is much faster. Because α_2 is faster than the competing rate β_3, the open channel (A_2R^*) has a much greater probability of closing than of reaching the second, more stable open state (A_2R^{**}). Thus, nonpolar or aromatic mutations dramatically impair the initial opening step in the gating pathway. Interestingly, αT422C shows a different behavior within this group of mutants; it is the only mutant in which the opening rate is much more affected than the closing rate. Comparison of rate constants of wild-type and M4 mutant AChRs, calculated on the basis of both Schemes I and II, confirms that αT422 contributes to channel opening and closing regardless of the kinetic scheme used for analysis. Scheme II was recently used to explain the activation of an AChR mutated in the M3 domain associated with a congenital myasthenic syndrome (Wang et al., 1999). This mutation, αV285I, also causes abnormally slow opening and rapid closing rates. Thus, Scheme II may represent a general mechanism that is not distinguished in wild-type AChR because the intermediate open state may be too short-lived to be detected, and the channel rapidly reaches the final open state. Thus, certain mutations that disrupt gating may have the ability to unmask intermediate open states.

The results also reveal the structural basis of the contribution of T422 to channel gating. Threonine and serine both contain polar hydroxyl groups, but differ by the presence of a methyl group attached to the beta carbon. Although the lack of a methyl group in serine slightly affects gating, αT422S AChRs are kinetically similar to wild-type AChRs. However, if only the hydroxyl group of threonine is replaced by a methyl group, as in valine, gating is substantially disrupted. Moreover, αT422V AChRs behave similarly to those containing structurally unrelated amino acids, such as tryptophan. The asparagine side chain provides similarly electronegative atoms to the original threonine side chain, and the polar amide group is similar to the hydroxyl group in its propensity for donating hydrogen bonds; T422N AChRs are almost kinetically identical to wild-type AChRs. Although cysteine can form hydrogen bonds, the kinetics of T422C AChRs differ from those of wild type. This finding can be explained by the fact that the thiol group is a poor hydrogen bond donor and forms weaker hydrogen bonds compared with hydroxyl or amide groups. Because hydroxyl and amide groups can equally well accept hydrogen bonds, and because, in contrast, cysteine is a poor hydrogen bond acceptor (Pal and Chakrabarti, 1998), an alternative interpretation would be that the side chain at position 422 acts as a hydrogen bond acceptor. In addition, the lower pKa of cysteine compared with threonine, or the greater hydrophobicity of cysteine compared with threonine, serine, or asparagine may contribute to the impaired channel gating. The observed gating kinetics of T422Y AChRs indicate that tyrosine does not provide the correct hydrogen bonding capability, perhaps owing to delocalization of electron density from the hydroxyl oxygen to the aromatic ring, or to the bulk of the aromatic ring. Interestingly, the tyrosine hydroxyl group is a poorer hydrogen-bond acceptor than an aliphatic or water hydroxyl group (Fersht et al., 1985). In summary, our results show that correct gating requires a hydrogen bond involving the side chain at position 422 in the M4 domain of the α subunit.

T422 is located in the last third of the M4 domain, closest to the outer leaflet of the bilayer (Fig. 4). Whether the M4 domain is an α helix (Blanton and Cohen, 1994) or a β-sheet (Unwin, 1993) remains controversial. In addition, current models of the AChR place M4 with a tilt of ∼30° with respect to the membrane (Ortells et al., 1997). Thus, atomic structure resolution of the AChR will be needed to unequivocally identify the hydrogen-bonding partner for αT422. Although T422 is labeled by the hydrophobic probe TID, and therefore is probably exposed to the lipid, its hydroxyl group could interact with a hydrogen bond acceptor or donor within a transmembrane domain of the same or another subunit. The more energetic hydrogen bonding expected in a hydrophobic environment may account for the substantial functional importance of the hydrogen bond with which T422 is involved. Thus, the present work demonstrates that subtle interactions originating far away from the two main functional domains of the AChR, the ion pore and the binding site, significantly affect channel gating.

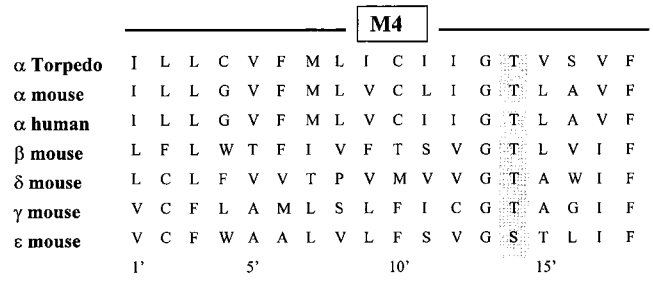

Figure 4. Sequence alignments of the M4 domains. The conserved T422 is shown as a shaded column.

Calculation of free energy changes for channel opening and closing disclosed only slight decreases in free energy for closing between serine and asparagine mutant AChRs, but revealed significant changes in free energy for both opening and closing steps for all other mutant AChRs. The free energy differences are on the order of those calculated for hydrogen bonds between uncharged residues in an aqueous solution (0.5–1.5 kcal/mol; Fersht et al., 1985), or for other weak interactions such as dipole–dipole interactions. Our observation that a hydrogen bond is required for proper gating agrees with the calculated free energy changes. However, the correlation between the free energy of a hydrogen bond and free energy of activation for a state transition is not necessarily strict, given that disruption of a chemical bond can have global consequences.

The significant role of a hydrogen bond at position 422 in channel gating demonstrated in the current work explains the high degree of conservation of T422 among subunits and species (Fig. 4). Abnormal activation of AChR has been shown to underlie congenital myasthenic syndromes (CMS) (Engel et al., 1998). Although mutations in the M4 domain have not been identified in CMS, our findings indicate that if they naturally occurred they could lead to a CMS.

Given the present understanding of the topology of the M4 domain, our results demonstrate that a lipid-exposed residue involved in hydrogen bonding is necessary for proper gating of the AChR.

We especially thank Dr. H.-L. Wang for advice and helpful discussion, Ana M. Roccamo, Dora Ortiz, and Horacio De Genaro for their expert technical assistance, and Nina Bren for providing two mutant subunits.

This work was supported by grants from Universidad Nacional del Sur, CONICET, and Agencia Nacional de Promoción Científica (C. Bouzat and F.J. Barrantes), National Institutes of Health grant NS-31744 (S. Sine), and Fogarty International Center grant 1R03 TW01185-01 (C. Bouzat and S. Sine).

Submitted: 6 December 1999
Revised: 27 March 2000
Accepted: 28 March 2000

REFERENCES

Akabas, M., and A. Karlin. 1995. Identification of acetylcholine receptor channel-lining residues in the M1 segment of the α-subunit. *Biochemistry.* 34:12496–12500.

Akk, G., and A. Auerbach. 1996. Inorganic, monovalent cations compete with agonists for the transmitter binding site of nicotinic acetylcholine receptors. *Biophys. J.* 70:2652–2658.

Blanton, M.P., and J.B Cohen. 1992. Mapping the lipid-exposed regions in the *Torpedo californica* nicotinic acetylcholine receptor. *Biochemistry.* 31:3738–3750

Blanton, M.P., and J.B. Cohen. 1994. Identifying the lipid-protein interface of the *Torpedo* nicotinic acetylcholine receptor: secondary structure implications. *Biochemistry.* 33:2859–2872.

Bouzat, C., N. Bren, and S.M. Sine. 1994. Structural basis of the different gating kinetics of fetal and adult nicotinic acetylcholine receptors. *Neuron*. 13:1395–1402.

Bouzat, C., A.M. Roccamo, I. Garbus, and F.J. Barrantes. 1998. Mutations at lipid-exposed residues of the acetylcholine receptor affect its gating kinetics. *Mol. Pharmacol*. 54:146–153.

Engel, A.G., K. Ohno, M. Milone, and S.M. Sine. 1998. Congenital myasthenic syndromes. New insights from molecular genetics and patch-clamp studies. *Ann. NY Acad. Sci. USA.* 841:140–156.

Fersht, A.R., J.-P. Shi, J. Knill-Jone, D.M. Lowe, A.J. Wilkinson, D.M. Blow, P. Brick, P. Carter, M.M.Y. Waye, and G. Winter. 1985. Hydrogen bonding and biological specificity analyzed by protein engineering. *Nature.* 314:235–238.

Hamill, O.P., A. Marty, E. Neher, B. Sakmann, and F.J. Sigworth. 1981. Improved patch-clamp techniques for high-resolution current recording from cells and cell-free membrane patches. *Pflügers Arch.* 391:85–100.

Lee, Y.H., L. Li, J. Lasalde, L. Rojas, M. McNamee, S.I. Ortiz-Miranda, and P. Pappone. 1994. Mutations in the M4 domain of *Torpedo californica* acetylcholine receptor dramatically alter ion channel fuinction. *Biophys. J.* 66:646–653.

Maconochie, D.J., and J.H. Steinbach. 1995. Block by acetylcholine of mouse muscle nicotinic receptors, stably expressed in fibroblasts. *J. Gen. Physiol.* 106:113–147.

Ortells, M.O., G.E. Barrantes, C. Wood, G.G. Lunt, and F.J. Barrantes. 1997. Molecular modelling of the nicotinic acetylcholine receptor transmembrane region in the open state. *Prot. Eng.* 10: 511–517.

Ortiz-Miranda, S.I., J.A. Lasalde, P.A. Pappone, and M.G. McNamee. 1997. Mutations in the M4 domain of the *Torpedo californica* nicotinic acetylcholine receptor alter channel opening and closing. *J. Membr. Biol.* 158:17–30.

Pal, D., and P. Chakrabarti. 1998. Different types of interactions involving cysteine sulfhydril group in proteins. *J. Biomol. Struct. Dyn*. 15:1059–1071.

Qin, F.A., A. Auerbach, and F. Sachs. 1996. Estimating single-channel kinetic parameters from idealized patch clamp data containing missed events. *Biophys. J.* 70:264–280.

Sakmann, B.J., J. Patlak, and E. Neher. 1980. Single acetylcholine-activated channels show burst-kinetics in the presence of desensitizing concentrations of agonist. *Nature*. 286:71–73.

Salamone, F.N., M. Zhou, and A. Auerbach. 1999. A re-examination of adult mouse nicotinic acetylcholine receptor channel activation kinetics. *J. Physiol*. 516:315–330.

Sigworth, F., and S.M. Sine. 1987. Data transformation for improved display and fitting of single-channel dwell time histograms. *Biophys. J.* 52:1047–1052

Sine, S.M. 1993. Molecular dissection of subunit interfaces in the acetylcholine receptor: identification of residues that determine curare selectivity. *Proc. Natl. Acad. Sci. USA*. 90:9436–9440.

Sine, S.M., K. Ohno, C. Bouzat, A. Auerbach, M. Milone, J.N. Pruitt, and A.G. Engel. 1995. Mutation of the acetylcholine receptor alpha subunit causes a slow-channel myathenic syndrome by enhancing agonist binding affinity. *Neuron*. 15:229–239.

Unwin, N. 1993. The nicotinic acetylcholine receptor at 9 Å resolution. *J. Membr. Biol.* 229:1101–1124.

Unwin, N. 1995. Acetylcholine receptor channel imaged in the open state. *Nature.* 373:37–43.

Wang, H.-L., A. Auerbach, N. Bren, K. Ohno, A.G. Engel, and S.M. Sine. 1997. Mutation in the M1 domain of the acetylcholine receptor α subunit decreases the rate of agonist dissociation. *J. Gen. Physiol.* 109:757–766.

Wang, H.-L., M. Milone, K. Ohno, X.-M. Shen, A. Tsujino, A.P. Batocchi, P. Tonali, J. Brengman, A.G. Engel, and S.M. Sine. 1999. Acetylcholine receptor M3 domain: stereochemical and volume contributions to channel gating. *Nat. Neurosci.* 2:226–233.